Tréhu, A.M., Bohrmann, G., Torres, M.E., and Colwell, F.S. (Eds.)
Proceedings of the Ocean Drilling Program, Scientific Results Volume 204

21. Data Report: Shapes and Structures of Gas Hydrates Imaged by Computed Tomographic Analyses, ODP Leg 204, Hydrate Ridge[1]

F. Abegg,[2] G. Bohrmann,[2] and W. Kuhs[3]

ABSTRACT

The sediments of Hydrate Ridge/Cascadia margin contain extensive amounts of gas hydrate. A total of 57 sediment samples including gas hydrate were preserved in liquid nitrogen and have been imaged using computerized tomography to visualize hydrate distribution and shape. The analysis gives evidence that gas hydrate in vein and veinlet structures is the predominant shape in the deeper gas hydrate stability zone with dipping angles from 30° to 90°(vertical).

INTRODUCTION

Gas hydrate samples obtained during Ocean Drilling Program (ODP) Leg 204 at Hydrate Ridge, Cascadia margin, represent a substantial set of hydrate specimens drilled during ODP. The samples cover a wide depth range of the gas hydrate stability zone (GHSZ) from the seafloor to almost 130 meters below seafloor (mbsf). Investigation of these samples considerably improves and broadens our understanding of the origin, structure, and distribution of hydrate within sediment deposits.

Because of the decomposition of hydrates under atmospheric conditions, nondestructive X-ray computed tomography (CT) (Orsi et al., 1992) offers a method of imaging preserved whole-round core samples to gain information on the shape, internal structure, and orientation of gas hydrates in their natural sedimentary environment. CT investiga-

[1] Abegg, F., Bohrmann, G., and Kuhs, W., 2006. Data report: Shapes and structures of gas hydrates imaged by computed tomographic analyses, ODP Leg 204, Hydrate Ridge. *In* Tréhu, A.M., Bohrmann, G., Torres, M.E., and Colwell, F.S. (Eds.), *Proc. ODP, Sci. Results,* 204, 1–11 [Online]. Available from World Wide Web: <http://www-odp.tamu.edu/publications/204_SR/VOLUME/CHAPTERS/122.PDF>. [Cited YYYY-MM-DD]
[2] Research Center Ocean Margins, University of Bremen, D-28334 Bremen, Germany. Correspondence author: **abegg@uni-bremen.de**
[3] GeoZentrum Göttingen, Abt. Kristallographie, University Göttingen, D-37077 Göttingen, Germany.

Initial receipt: 3 May 2005
Acceptance: 4 April 2006
Web publication: 26 September 2006
Ms 204SR-122

tions on natural marine gas hydrates have previously been conducted by Uchida et al. (1997) on samples from Blake Ridge (ODP Leg 164). The major conclusion of their study was that medical CT instrumentation can distinguish gas hydrate from the surrounding matrix and determine its structure and interbedding with the sedimentary matrix.

Over the last two decades and during Leg 204 (e.g., Malone, 1985; Shipboard Scientific Party, 2003), scientists introduced several terms describing differences in hydrate fabric and outline shapes. Leg 204 shipboard scientists used thermal shapes imaged by infrared (IR) camera measurements to determine hydrate morphology in the sediment. During this study we used CT imaging on preserved hydrate-bearing sediment samples.

SAMPLES AND METHODS

The gas hydrate sampling procedure on board the *JOIDES Resolution* utilized results from the IR camera monitoring and visual observations of gas hydrate presence in the cores examined on the catwalk (Tréhu, Bohrmann, Rack, Torres, et al., 2003). Whole-round sediment sections of variable length (~5–20 cm) were taken from samples identified by such methods and then were immediately transferred into sample bags and stored in liquid nitrogen on the catwalk to avoid further dissociation by putting the hydrate into the GHSZ. We used a total of 65 such preserved samples to perform our analyses, including one triplicate and six duplicate samples, resulting in 57 samples from different sites and depth levels (see Table **T1**).

For CT investigation of the frozen samples we used a MARCONI Medical MX 8000 CT scanner located in a radiological clinic (Gemeinschaftspraxis Pruener Gang, Kiel, Germany). CT slices were 1 mm thick, and the field of view of 90 mm × 90 mm was covered by a data matrix of 512 × 512 pixels. The resulting voxel size was 0.03 mm^3.

During CT scans the hydrates were placed on a socket inside a foam box. The foam box was filled with a thin layer of liquid nitrogen in order to stabilize the hydrate within the GHSZ.

PRELIMINARY RESULTS AND DISCUSSION

Gas hydrates in the samples were classified from the CT images based upon their shape. The results are listed in the Table **T1** as "CT shape." The classification is generally sourced on terms that have been defined for the description of hydrates visualized by thermal imaging using IR cameras (Tréhu, Bohrmann, Rack, Torres, et al., 2003; J.L. Weinberger, pers. comm., 2005). The IR method uses the endothermic dissociation of hydrate, which forms cold thermal anomalies on the core liner. Such defined IR shapes are listed in Table **T1** for comparison.

The following fabric types, listed from small to large hydrate features, were identified on the CT images (see **"Supplementary Material"** for CT images):

1. Disseminated hydrate (Fig. **F1**): smallest pieces of gas hydrate with grain sizes up to 3 mm, which are disseminated in the sediment; such hydrate grains are not connected. Sometimes grains are hardly visible, which may partly be due to dissociation during recovery. Based on their small mass, such grains dissociate

T1. Fabric analyses based on CT imaging, p. 11.

F1. CT slice, gas, and gas hydrate, p. 6.

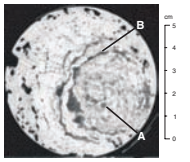

very rapidly after leaving the gas hydrate stability field in comparison to hydrate pieces of larger size.

2. Veinlet (Fig. F1): thin tabular hydrate, 1 mm thick in different orientations. Veinlets can appear as disks in three dimensions and thus are the small or thin form of veins.
3. Vein (Fig. F2): similar to veinlets but differ in thickness from 1 mm up to 10 cm. Veins, as well as veinlets, are nonparallel to bedding planes and transect the sedimentary bedding. The dip angle varies from nearly horizontal to vertical. Analyzing the dip angles of veins, it is obvious that almost all angles are >30° with a tendency to angles >60°.
4. Layer (Fig. F3): differs from veins because of the orientation in the sediment: a layer transects the core conformably to bedding. Hydrate layers are often intercalated between fine-grained sediment layers.
5. Nodule (Fig. F4): spherical to oblate features, typically 1–5 cm in diameter, sometimes with edges.
6. Massive hydrate (Fig. F5): thicker than ~10 cm and less than ~25% intercalated sediment.

In many cases the difference between such defined shapes is based only on the orientation of the hydrate within the sedimentary bedding. An important example: veins and layers are comparable in size, but veins cross the bedding planes and layers are intercalated among horizontal sediment layers. In this study we did not use the term "lens" because the sample size was too small to observe a tapering margin. Nodules sometimes look like small lenses. They are described as spherical to oblate, and if their size exceeds the core diameter they appear as layers. Furthermore, massive hydrate may also represent a layer parallel to bedding, which on a larger scale most probably looks like a lens.

Other features often observed are bubble fabrics in which the bubble size and the density of bubbles vary. A bubble fabric often occurs in the outer part of the core slices (Fig. F1) and is caused by the formation of gas bubbles in a soupy sediment that results from the dissociation of hydrate during core recovery and the sampling procedure on the catwalk. Because the samples were immediately frozen in liquid nitrogen, the bubbles were conserved.

The density of the frozen mud containing the bubbles is higher than the density of hydrate but lower than the ambient sedimentary matrix. Disseminated hydrate seems to be particularly susceptible to rapid hydrate dissociation. Because of the effective water release from such hydrate, dissociation of disseminated hydrates in fine-grained sediments leads to the formation of soupy sediments where gas bubbles are constantly being released. Very often this results in soft-sediment deformation of various dimensions (Fig. F1). Small amounts of gas are released when pressure reduction reduces solubility.

Based on our CT analyses, hydrate from deeper in the GHSZ predominantly appears as veins or veinlets with dipping angles of >30°, which are fracture or channel fillings that occurred in the sediment sequence because of tectonic movements of Hydrate Ridge. Sometimes before these fractures were filled completely by hydrate, they were filled in situ by fluids or free gas and may represent structures through which free gas could move rapidly through the sediment column to the surface. The mechanism for supply of free gas from a horizon characterized as Reflector A from beneath the bottom-simulating reflector (BSR) and the transport mechanism through the GHSZ has been described by Tréhu et

F2. Hydrate resembling vein, p. 7.

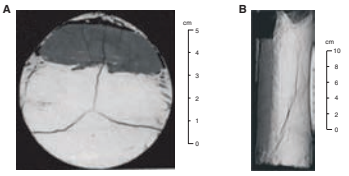

F3. Gas hydrate layer, p. 8.

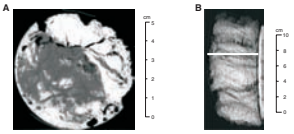

F4. Hydrate nodules, p. 9.

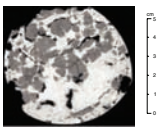

F5. Massive hydrate, p. 10.

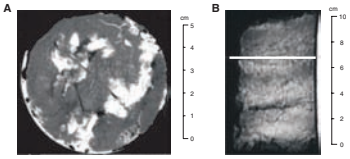

al. (2004). Free gas discharge from the seafloor into the water column of southern Hydrate Ridge has also been observed during various cruises (e.g., Suess et al, 1999; Heeschen et al., 2003). The rim of these channels or fractures within the GHSZ may be stabilized by hydrate formation at the sediment/gas interface and may explain why free gas can move upward away from any water contact. After the decrease of gas flow, the hydrate filled up the entire volume of the inner part of the channel or fracture. An example of such a steep-dipping vein is given in Figure F2B. The visible length of the x-axis of this hydrate vein (Section 204-1248C-10H-1) reached a length of 13.5 cm. Adding another 4.8 cm, measured on a subsample, it sums to a length of >18 cm, which is still not the total length because top and bottom have not been preserved.

ACKNOWLEDGMENTS

This research used samples and data provided by the Ocean Drilling Program (ODP). ODP is sponsored by the U.S. National Science Foundation (NSF) and participating countries under management of Joint Oceanographic Institutions (JOI). Funding for this research was provided by Deutsche Forschungsgemeinschaft (DFG Grant BO 1049/7 and KU 920/13). We also thank Mrs. Kornelia Graef for her assistance in CT scanning.

REFERENCES

Heeschen, K.U., Tréhu, A.M., Collier, R.W., Suess, E., and Rehder, G., 2003. Distribution and height of methane bubble plumes on the Cascadia margin characterized by acoustic imaging. *Geophys. Res. Lett.,* 30:1643–1646. **doi:10.1029/2003GL016974**

Malone, R., 1985. *Gas Hydrates Topical Report–DOE/METC/SP-218* (DE85001986): Morgantown (DOE, Morgantown Energy Technology Center).

Orsi, T.H., Anderson, A.L., Leonard, J.N., Bryant, W.R., and Edwards, C.M., 1992. Use of X-ray computed tomography in the study of marine sediments. *Proc. Int. Conf. Civ. Eng. Oceans,* 968–981.

Tréhu, A.M, Bohrmann, G., Rack, F.R., Torres, M.E., et al., 2003. *Proc. ODP, Init. Repts.,* 204 [Online]. Available from World Wide Web: <**http://www-odp.tamu.edu/publications/204_IR/204ir.htm**>. [Cited 2004-02-03]

Tréhu, A.M., Flemings, P.B., Bangs, N.L., Chevallier, J., Gràcia, E., Johnson, J.E., Liu, C.S., Liu, X., Riedel, M., and Torres, M.E., 2004. Feeding methane vents and gas hydrate deposits at south Hydrate Ridge. *Geophys. Res. Lett.,* 31:L23310. **doi:10.1029/2004GL021286**

Shipboard Scientific Party, 2003. Explanatory notes. *In* Tréhu, A.M, Bohrmann, G., Rack, F.R., Torres, M.E., et al., *Proc. ODP, Init. Repts.,* 204, 1–102 [CD-ROM]. Available from: Ocean Drilling Program, Texas A&M University, College Station TX 77845-9547, USA. [**HTML**]

Suess, E., Torres, M.E., Bohrmann, G., Collier, R.W., Greinert, J., Linke, P., Rehder, G., Tréhu, A., Wallmann, K., Winckler, G., and Zuleger, E., 1999. Gas hydrate destabilization: enhanced dewatering, benthic material turnover, and large methane plumes at the Cascadia convergent margin. *Earth Planet. Sci. Lett.,* 170:1–15. **doi:10.1016/S0012-821X(99)00092-8**

Uchida, T., Yamamoto, J., Okada, S., Waseda, A., and Okatsu, K., 1997. Characteristics of natural methane hydrates obtained from ODP Leg 164: X-ray CT, NMR and geochemical investigations. *Int. Conf. Nat. Gas. Hydrates, 3rd,* 27–33.

Figure F1. CT slice is a negative, dense material displayed in white (Sample 204-1249C-2H-1, 108–140 cm). Black = gas, dark gray = gas hydrate. Hydrate concentrates on the lower right side of the core. A = grain of hydrate, B = concentric structures comparable to veinlets. Sediment outside of this structure encloses gas bubbles (black), which are likely to be generated during core recovery because of their alignment to the margin of the core.

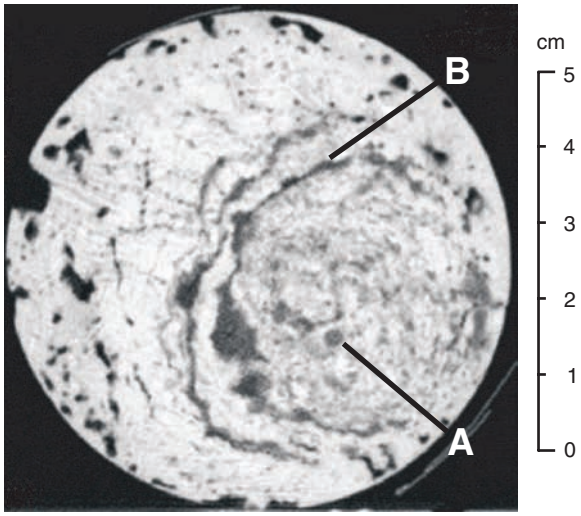

Figure F2. A. Hydrate looks like a large vein in cross section (Sample 204-1248C-10H-1, 100–119 cm). Width and breadth (2 cm × 5.5 cm) only provides an estimate because it seems that the some of the hydrate has been cut off during the coring process. **B.** Two-dimensional overview (Sample 204-1248C-10H-1, 100–119 cm). The "vein," steeply dipping, has an extension of ~13.5 cm along the core axis. Adding the length of a subsample, the total length of the vein sums up to >18 cm.

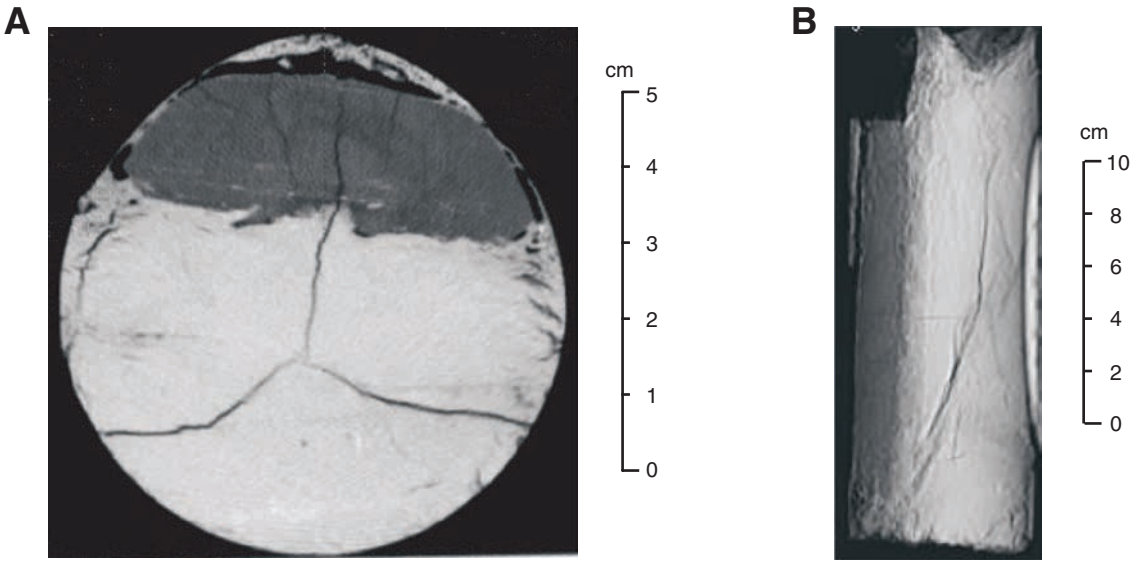

Figure F3. A. Gas hydrate layer with sediment and bubble fabric (Sample 204-1249C-1H-1, 25–55 cm). **B**. Two-dimensional overview presents layer structure (Sample 204-1249C-1H-1, 25–55 cm). White line = location of slice in A.

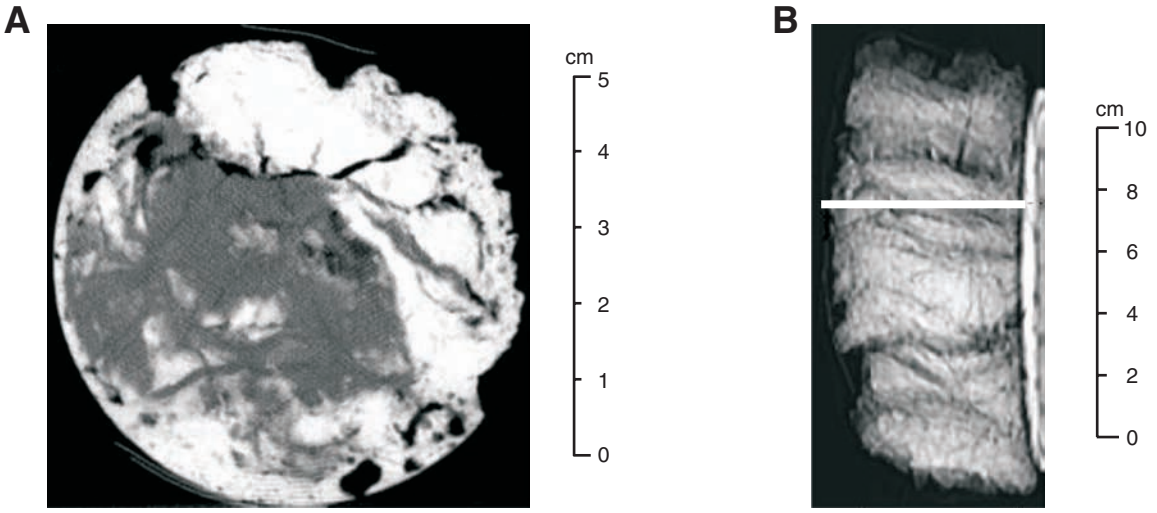

Figure F4. Hydrate nodules of different sizes (Sample 204-1248C-8H-6, 68–87 cm). Besides spherical shapes there are also some nodules with well-defined edges.

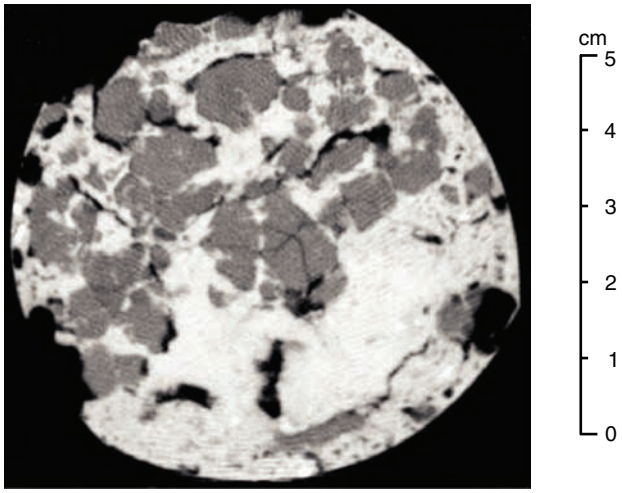

Figure F5. A. Gas hydrate spreads over the rims in this example of a massive hydrate (Sample 204-1249C-1H1, 0–25 cm). Some sediment is intercalated. **B.** Two-dimensional overview shows extent of hydrate and variation in amount of intercalated sediment (Sample 204-1249C-1H1, 0–25 cm).

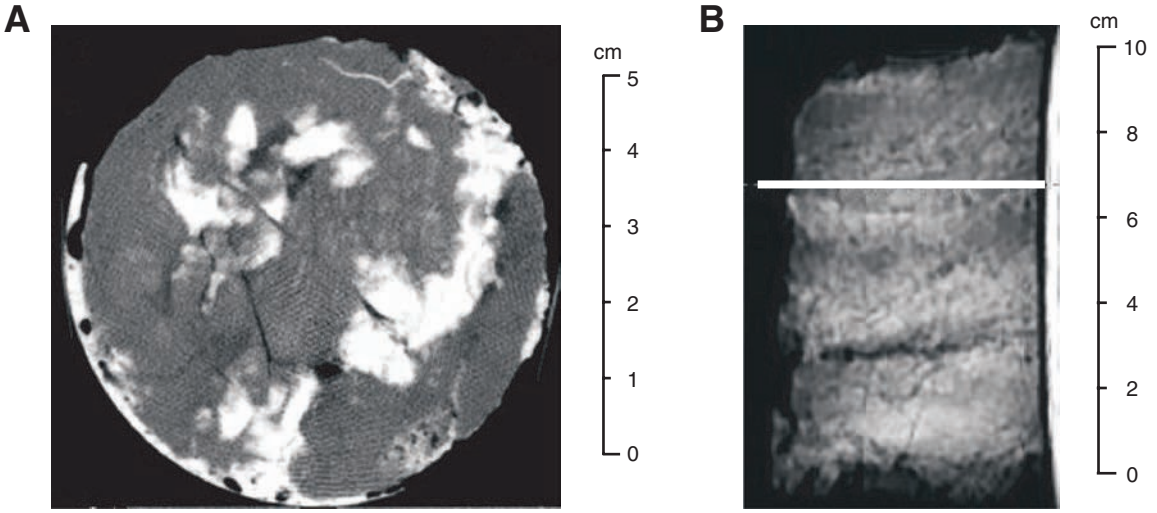

Table T1. Results from fabric analyses based on computed tomographic imagining, listed as computed tomographic shapes.

Hole, core, section, interval (cm)	Depth (mbsf)	Computed tomographic shape	Vein angle (°)	Infrared shape
204-				
1244C-8H-1, 47–52	62.97	Vein, small sample		Nodular; vein
1244E-12H-1, 50–60	74.10	Vein, veinlets, bubble fabric	60–90	Nodular
1244C-10H-2, 70–103	83.70	Vein, veinlets, bubble fabric	0–30, 30–60	Nodular; vein; steep dip; 2-cm nodules
1244E-13H-6, 107–150	90.97	Vein, veinlets	30–60	Vein; thick; steep dip; nodular
1245B-6H-5, 60–78	54.10	Vein, small sample		Nodular on deeply dipping plane
1245B-7H-1, 44–55	57.44	Vein, veinlets, bubble fabric	60–90	Nodular; two separate pieces
1245C-10H-2, 40–55	70.32	Irregular veinlets		Nodular
1245C-10H-5, 99–109	74.38	Undefined		Vein; low dip sharp top, gradational bottom
1245C-11H-2, 52–72	79.60	Disseminated, bubble fabric		Nodular
1245C-14H-5, 125–135	113.75	Gas hydrate not obvious		Vein parallel to bedding
1245C-15X-1, 28–64	116.28	Gas hydrate not obvious		Nodular, core top hydrate sample missing
1245B-15X-2, 0–10	129.26	Undefined		Nodular, adjacent to void and steeply dipping fracture
1246B-11H-5, 93–126	96.65	Sample disturbed, veinlets		Vein
1246B-13H-1, 0–30	109.20	Bubble fabric		Nodular
1247B-12H-2, 41–51	93.01	Vein	60–90	Nodular
1248C-1X-CC, 0–14	2.24	Veinlets, vein, disseminated, small sample		
1248B-2H-2, 0–25	7.37	Veinlet, small sample		
1248C-3X-3, 0–3	21.83	Layer, veinlets, small sample		
1248C-6H-2, 48–53	49.71	Small sample, no CT		Disseminated
1248C-8H-6, 68–87	74.46	Nodular, vein, bubble fabric	30–60	Nodular
1248C-10H-1, 100–119	87.00	Vein	60–90	Nodular
1248C-11H-5, 38–75	100.89	Vein	60–90	Disseminated
1248C-12H-4, 105–115	110.51	Vein, layer	60–90	Nodular; disseminated
1249C-1H-1, 0–25	0.00	Massive		
1249C-1H-1, 25–55	0.25	Layer, bubble fabric		
1249C-1H-1, 125–142	1.25	Vein, veinlets, sample disturbed		
1249C-1H-CC, 0–10	1.50	Layer, bubble fabric		
1249C-1H-CC, 0–10	1.50	Layer-massive, bubble fabric		
1249C-2H-1, 108–140	2.91	Veinlets, disseminated, bubble fabric		
1249C-3H-1, 88–106	5.89	Disseminated, bubble fabric		
1249C-3H-1, 106–131	5.89	Disseminated, veinlets, bubble fabric		
1249C-3H-CC	7.15	Veinlets, bubble fabric, sample disturbed		
1249F-3H-1, 8–10	11.03	Nodular-massive, small sample		Nodular
1249F-5H-1, 64–70	16.14	Veinlets, bubble fabric		
1249B-2A-1, 70–80	30.60	Layer, bubble fabric		
1249B-2A-2, 126–141	31.96	Disseminated, bubble fabric		
1249B-3A-1, 46–55	34.86	Veinlets, bubble fabric		
1249C-7H-1, 86–96	35.86	Veinlets, bubble fabric, sample disturbed		
1249C-7H-2, 87–97	36.83	Disseminated, bubble fabric		
1249C-7H-3, 22–33	37.15	Layer, veinlets, bubble fabric		
1249B-4H-1, 45–53	39.35	Gas hydrate not obvious		
1249C-8H-3, 0–18	47.46	Veinlets		
1249B-6A-1, 83–95	47.90	Veinlets, bubble fabric		
1249C-8H-4, 139–152	50.33	Gas hydrate not obvious		
1249F-10H-5, 86–106	55.66	Vein, bubble fabric	60–90	Steeply dipping vein
1249C-11H-4, 119–129	69.32	Gas hydrate not obvious		
1249C-12H-1, 110–120	75.60	Vein, bubble fabric	60–90	
1250D-1H-3, 30–63	1.66	Massive		
1250D-1H-CC, 0–14	2.57	Layer, small sample		
1250C-2H-1, 0–56	4.50	Layer, bubble fabric, sample disturbed		
1250C-2H-CC, 0–1	5.06	Veinlets, nodular, bubble fabric		
1250C-4H-3, 100–110	27.50	Vein, veinlets, sample disturbed		Vein; nodular
1250D-10H-3, 53–84	78.01	Vein, veinlets, nodular, bubble fabric	30–60	Vein; dipping
1250C-11H-3, 94–95	86.35	Vein, small sample		
1250C-12H-1, 50–51	92.50	? nodular, small sample		
1250F-1H-1, 23–33	100.23	No CT, sample too small		
1252A-11H-1, 70–80	98.60	Veinlets, vein, bubble fabric	0–30	

Notes: Infrared shapes from thermal imaging (Tréhu, Bohrmann, Rack, Torres, et al., 2003) are shown for comparison. Vein angle = dipping angle of veins. CT = computed tomography.